Iranian Journal of Science and Technology, Transactions of Mechanical Engineering (2025) 49:1773–1789
https://doi.org/10.1007/s40997-025-00874-2

RESEARCH PAPER

# A Hybrid Piezoelectric-Electromagnetic Wind Energy Harvester: Influence of Undisturbed Vorticity Formation on Performance

**Abdul Saboor[1] · Kangokar Nithin[1] · Muhammad Hafizh[2] · Mohammad Farhan[1] · Asan G. A. Muthalif[1]**

Received: 19 December 2024 / Accepted: 17 April 2025 / Published online: 8 May 2025


**Abstract**
The performance of a hybrid piezoelectric-electromagnetic-based wind energy harvester (HPEWEH) is presented in this article. Wind flow over a bluff body produces vortex-induced vibration (VIV), which is harvested simultaneously via a piezoelectric patch and an electromagnet. The orientation of HPEWEH is crucial for directing undisturbed wind flow and vortex formation. The hybrid piezoelectric-electromagnetic harvester integrates two electromechanical transduction systems: a piezoelectric macro-fiber composite and an electromagnetic mechanism. These systems are coupled via a bluff body, which is excited by vortex-induced vibrations (VIV), enabling simultaneous energy conversion from mechanical oscillations. The piezoelectric composite is bonded to a substrate beam to convert the mechanical strain into electricity. Additionally, electricity is produced in the electromagnetic section by converting changes into magnetic flux inside a container made from two slits that are wrapped with coils. A simulation study is conducted using ANSYS Fluent to investigate turbulence in the two configurations. In Configuration A, the bluff body faces the incoming wind, with the beam positioned behind it in the wake region. Conversely, Configuration B has the beam at the front, followed by the bluff body in the wake region. It is found that configuration B allows for the undisturbed production of vortices, resulting in a 33% greater gain in turbulent energy. Moreover, a larger output voltage is produced during frequency synchronization because, under synchronization, the vortex-shedding frequency and the structure's natural frequency are the same. The maximum voltage output occurs in this region, with configuration B producing 15% more voltage output than configuration A.

**Keywords** Hybrid energy harvesting · Piezoelectric · Electromagnetic · Vortex-induced vibration · Wind energy

## 1 Introduction

Implementing the Internet of Things (IoT) and machine learning for fault diagnosis can enhance decision-making and optimize asset integrity. However, powering these systems continuously, especially in remote installations without access to the main power supply, presents a challenge. Although fixed-energy–density batteries are typically employed, their short lifespan and the need for frequent replacements render them unsustainable (Tran et al. 2022; Shirazi and Jafari 2024). As technology becomes more efficient and energy harvesting methods advance, there is a growing opportunity to enhance the sustainability of both energy utilization and the lifespan of devices. Technologies such as piezoelectric, triboelectric, and electromagnetic energy harvesting have gained significant attention as sustainable solutions for converting ambient mechanical energy into electrical energy. One such promising development is in the field of piezoelectric energy harvesting (PEH), which has been the focus of substantial research and innovation in recent years (Chakhari et al. 2023). PEH is valued for efficiently converting kinetic energy into electrical power and storing it in batteries or capacitors (Sodano et al. 2005; Farhan et al. 2024). Prior studies have yielded valuable insights concerning the optimal design of piezoelectric energy harvesting systems and the underlying driving mechanisms associated with such designs (Muthalif and Nordin 2015; Kianpoor and Jahani 2019). As an environmentally friendly and renewable energy resource, wind power is both ecologically sound and abundantly available in the natural surroundings (Lin et al. 2019).

✉ Asan G. A. Muthalif
drasan@qu.edu.qa

[1] Department of Mechanical and Industrial Engineering, College of Engineering, Qatar University, 2713 Doha, Qatar

[2] School of Mechanical, Aerospace and Civil Engineering, University of Sheffield, Mappin Street, Sheffield S1 3JD, UK

One of the most common methods to harvest vibration energy is vortex-induced vibration (VIV), in which the vibration energy harvester is excited by periodic oscillations produced by vortex-shedding (Wang and Duan 2024). Flow-induced vibrations have several forms, including fluttering, galloping, and buffeting. The effectiveness of a piezoelectric energy harvester can be further enhanced by adding a bluff body, which enables energy harvesting through flow-induced vibration of an incoming fluid, such as wind (Song et al. 2016). By mounting piezoelectric beams to bluff bodies, vortex-induced vibration energy harvesting advances upon traditional piezoelectric energy harvesting (Gabbai and Benaroya 2005). Incorporating a bluff body that is cylindrically shaped has been observed to enhance the deflection of the piezoelectric beam by leveraging the extensively studied phenomenon of vortex-induced vibrations (VIVs) (Bearman 2011; Zhao 2023). Incorporating a tip mass into the cylindrical bluff body introduces an additional design parameter that can be utilized to adjust the resonance frequency, thereby optimizing the power output to its maximum value (Pradeesh and Udhayakumar 2019). Proposed mathematical models have been demonstrated to exhibit a strong correlation with experimental data in describing the behavior of a cylindrical bluff body subjected to vortex-induced vibration (Blevins 2009).

An examination was conducted to investigate the utilization of a piezoelectric cantilever featuring a cylindrical extension in harnessing flow-induced vibrations (FIV) near its natural frequency. The study's findings led to the conclusion that the resultant voltage output in turbulent flow conditions would be satisfactory for powering small-scale electronic equipment (Gao et al. 2013). This phenomenon results from harnessing energy from fluid flow, which leads to recurrent oscillations characteristic of the von Karman vortices. It has been observed that conversion efficiency increases as the harvester's size decreases, primarily due to the oscillation frequency (Pobering et al. 2009). The current literature has witnessed an increase in the implementation of piezoelectric energy harvesting (PEH) due to its outstanding performance, adaptability, and compactness at a reasonable cost (Safaei et al. 2019; Elahi et al. 2018). The piezoelectric patches are mounted on beams that have the ability to oscillate and produce a charge when mechanically strained. The literature's optimization study has revealed parameter insights for maximizing voltage output (Fakhzan and Muthalif 2013). Although they have lower power density than other energy harvesting methods, piezoelectric energy harvesters are highly efficient, offer a good cost-to-performance ratio, and can be utilized in various vibration energy harvesting applications (Jiang et al. 2020). Piezoelectric materials are, therefore, utilized in many sectors for wireless sensor powering and condition monitoring purposes (Lu et al. 2021). While electromagnetic generators are used in energy harvesting, they are often only utilized in bigger systems due to their bulkier nature than piezoelectric generators alone (Beeby et al. 2006; Esalat et al. 2023). A hybrid energy harvester can extract energy from both piezoelectric and electromagnetic systems. It has recently been demonstrated that these hybrid systems perform better than traditional piezoelectric energy harvesters that employ either macro fiber composites (MFC) or monolithic piezoelectric (PZT) (Lai et al. 2021). When the vortex shedding frequency coincides with the structural natural frequency during synchronization, the voltage output from this energy harvesting approach has been demonstrated to achieve its maximum (Konstantinidis et al. 2021; Nishi and Shigeyoshi 2022). By exploiting vortex shedding and synchronization, optimization parameters for these energy harvesters have been established (Dalton 2010; Williamson and Govardhan 2008). Moreover, Akaydin et al. (2012), illustrated the significance of coupling aerodynamic, electrical, and mechanical factors, which substantially influence power generation, damping, and electrical resistance. Research in combined flow-induced vibration (FIV) energy harvesters has seen notable developments.

Moreover, incorporating an external electromagnetic oscillator in tandem with a piezoelectric harvesting beam holds the potential to increase the system's power output by as much as 30% (Challa et al. 2009). Similarly, Zhao et al. (2017) proposed a combined hybrid system in which FIV oscillations can harvest energy through electromagnetic induction and piezoelectric strain, resulting in a greater total output. In addition, Zhang et al. (2017) showed that utilizing magnetic forces to harvest broadband energy through VIV could increase the synchronization region by approximately 140% and the harvester power level by around 30%. Similarly, Challa et al. (2009) reported that the power output of a standard piezoelectric energy harvester was enhanced by 30% upon the incorporation of an electromagnetic harvester. The work of Hafizh et al. (2021) and Muthalif et al. (2021) has shown novel designs of hybrid harvesters, which have various optimizations of the components of the bluff body. In particular, the dual-mass type of harvester showed an improvement in the output voltage of around 50%. Due to their ability to be adjusted for varying frequency ranges, hybrid energy harvesters consist of numerous systems that are appropriate for broadband applications (Ibrahim et al. 2017). Despite extensive research on hybrid piezoelectric-electromagnetic energy harvesters, most existing designs primarily focus on material selection, frequency tuning, and energy conversion mechanisms while often overlooking the critical role of spatial configurations in optimizing vortex-induced vibration (VIV) efficiency. The arrangement of structural elements within the flow field has a significant impact on vortex formation, shedding patterns, and wake interactions, which directly influence the amplitude and stability of induced vibrations. When spatial configurations

are not optimized, wake interference between components can dampen vortical structures and reduce turbulent kinetic energy, ultimately limiting voltage output.

Addressing this overlooked aspect, our study emphasizes the importance of spatial design as a key parameter for enhancing the aerodynamic response and maximizing energy harvesting efficiency in hybrid systems. This paper presents a unique design of a hybrid energy harvester that employs the collection of power from incoming wind streams through the vibration of a piezoelectric patch and an electromagnetic oscillator. The goal is to maximize the power output of the harvester, especially during synchronization tuning. Therefore, studies are conducted to determine the optimal configuration relative to the wind flow. Moreover, the selection of two configurations (A and B) was guided by the need to explore the influence of wake interference on turbulence generation and energy harvesting efficiency. In contrast, the designs of wind energy systems currently in use have been well researched, our attention to the particular spatial arrangements of the beam and bluff body aims to reveal subtleties in the mechanics of vortex shedding.

## 2 Mathematical Modelling of Hybrid Harvester

The mathematical model of a piezoelectric-electromagnetic hybrid energy harvester was developed. The harvester's dynamic model is shown as it is positioned in a wind tunnel. For piezoelectric and electromagnetic systems, vortex-induced vibrations result in bluff body oscillations that generate electricity. Lastly, a synchronization model is developed to show the effect of synchronization of the natural frequency.

### 2.1 Hybrid Energy Harvesting

The design of the energy harvester and the inside view are shown in Fig. 1, with a macro-fiber composite/piezoelectric patch bonded to a beam attached to a cylindrical bluff body. The empty space inside the bluff body is filled by putting the EM harvester inside, constrained by two slits. Transverse vibrations are caused by the beam attached to the bluff body oscillating perpendicular to the direction of the incoming wind flow, which flows around the harvester. An elastically supported discrete system can be used to model the main deformation (Franzini and Bunzel 2018; Facchinetti et al. 2004). The mathematical model, as seen in Fig. 2, is derived from the discrete system because the highest harvester performance is dependent on its natural frequency tuning. Three neodymium bar magnets were employed to enhance the energy obtained from the internal electromagnetic harvester (Roundy and Wright 2004; Jia et al. 2018). These were suspended between two neodymium disk-shaped magnets at the top and three at the bottom to account for the effects of gravity. To decrease contact friction during sliding movements, high grit sandpaper was used to smoothen the insides of the slits. Natural frequency tuning was also made possible by the modular design, which allowed for the addition or removal of masses. The accuracy of the mathematical

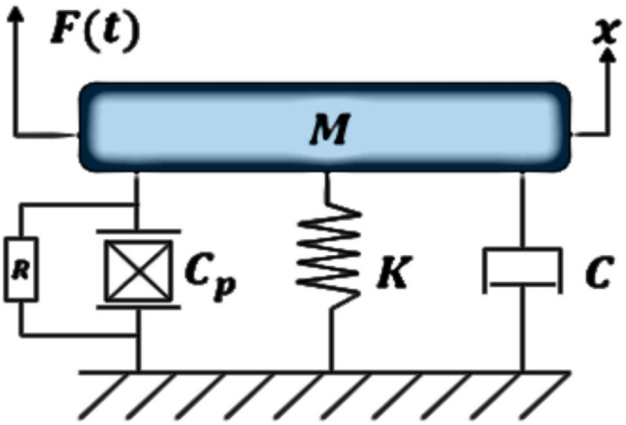


**Fig. 2.** Equivalent system of setup

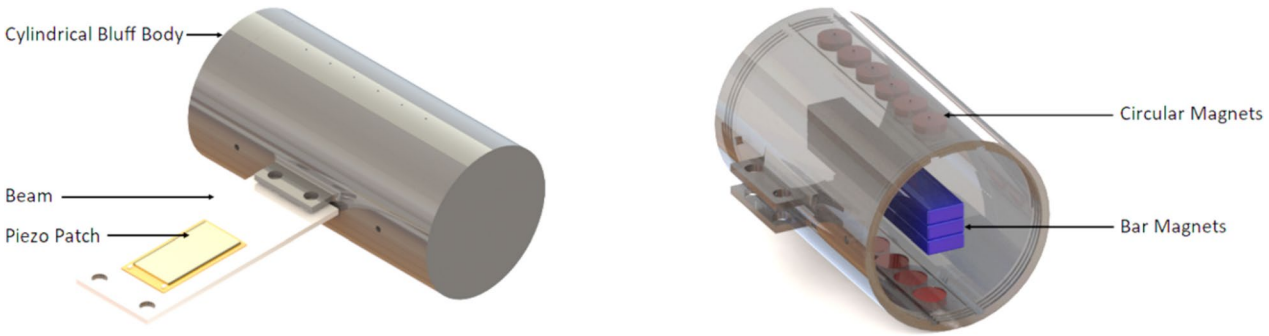


**Fig. 1** Setup of hybrid harvester

model relies on the precise determination of parameters, some of which could be subject to inherent uncertainties.

Due to the von Karman effect, vortices will develop after the cylindrical bluff body, causing oscillations in a direction transverse to the wind flow. A mass-spring-damper system can describe these oscillations, which are stated in terms of time in Eq. (1) (Muthalif et al. 2021).

$$M\ddot{x} + C\dot{x} + Kx + \Theta V_p = F(t) \tag{1}$$

In this equation, $M$ represents the equivalent mass, $C$ represents the equivalent damping, and $K$ represents the equivalent stiffness. The effect of the piezoelectric patch once strained is represented by $\Theta$, which is the electromechanical coupling coefficient, and $V_p$ is the corresponding output voltage. There is a current induced from the piezoelectric patch, which can be represented by $I_p$, in Eq. (2)

$$I_p = \frac{V_p}{R} = \Theta\dot{x} - C_p\dot{V}_p \tag{2}$$

where $R$ is the resistive load, and $C_p$ represents the piezoelectric transducer capacitance. Furthermore, the bluff body's electromagnetic oscillator system produces electricity by electromagnetic induction. The transverse vortex-shedding force is expressed as $F_T$, which can be expressed as the product of the velocity and inertia coupling coefficients (Bearman 2011). Equation (3) can be utilized to explain the vortex-shedding-induced transverse oscillations.

$$F_T = \frac{\rho U^2 DL\left(C_{mv}\sin(2\pi ft) + C_{dv}\cos(2\pi ft)\right)}{2} \tag{3}$$

where $f$ is the frequency of oscillation of the cylinder, $D$ is the bluff body diameter, $\rho$ is the moving fluid density, $U$ is the freestream velocity of the fluid, $L$ is the length of the cylinder's surface that is in contact with the fluid (wetted length), $C_{mv}$ is a coefficient that represents the inertia of oscillation and $C_{dv}\,C_{dv}\,C_{dv}$ is a coefficient that represents the negative damping coefficient.

## 2.2 Synchronizing Harvester

It is advantageous to harvest energy at natural frequency to improve the performance of vibration-based energy harvesting systems that use an electromagnetic oscillator and a piezoelectric system for narrowband applications. This is because the strain on the piezoelectric material generates the most electrical charge, while the magnet's movement produces the most current. The representation of the natural frequency of a discrete system in an air medium is shown in Eqs. (4–6) (Muthalif et al. 2022).

$$\omega_n = \sqrt{\frac{K}{M}} \tag{4}$$

$$\omega_d = \omega_n\sqrt{1-\zeta^2} \tag{5}$$

$$\zeta = \frac{C}{2\sqrt{KM}} \tag{6}$$

In these equations, $\omega_n$ is the natural frequency, $K$ is the stiffness, $M$ is the mass, $\omega_d$ is the damped natural frequency, $\zeta\,\zeta\,\zeta$ is the damping ratio, and $C$ is the damping coefficient.

To achieve optimal performance, it is crucial to tune the energy harvester to the desired free stream velocity during the harvester's design phase. Calculating this synchronization can be approximated by utilizing the Strouhal number, which describes the oscillating system involved, as shown in Eq. (7) (Norberg 2003).

$$St = \frac{f_s \cdot D}{U} \tag{7}$$

where $S_t$ represents the Strouhal number, $f_s$ is the frequency of vortex shedding, $D$ is the diameter of the cylinder, and $U$ is the free-stream velocity.

The root mean square (RMS) method is employed to assess the energy harvesting system's performance and compare the two different configurations. Equation (8) allows for a unified evaluation of the harvester's output. The RMS voltage serves as a standardized measure to quantify the overall performance of the energy harvesting system under consideration.

## 2.3 CFD Simulation Study

In the process of modeling a hybrid energy harvester inside a wind tunnel using computational fluid dynamics (CFD), a 2D approach was employed to visualize the effects of vortex shedding and wake generation across the cylindrical bluff body in two different configurations (Hafizh et al. 2021). The computational domain consisted of a velocity inlet of wind at a speed nearing the synchronization speed, as well as 20$D$ non-slip boundary walls, where $D$ represents the diameter of 50 mm of the circular bluff body measured from its center and 10$D$ upstream. To allow for wake generation and the visualization of vortex shedding over a period of 15 s, the total length of the domain was modeled as 30$D$. The top and bottom of the boundary were treated as no-slip zones, while the outlet boundary was given a static pressure of zero Pa. The computational domain and mesh distribution around the cylindrical bluff body are illustrated in Figs. 3 and 4, respectively.

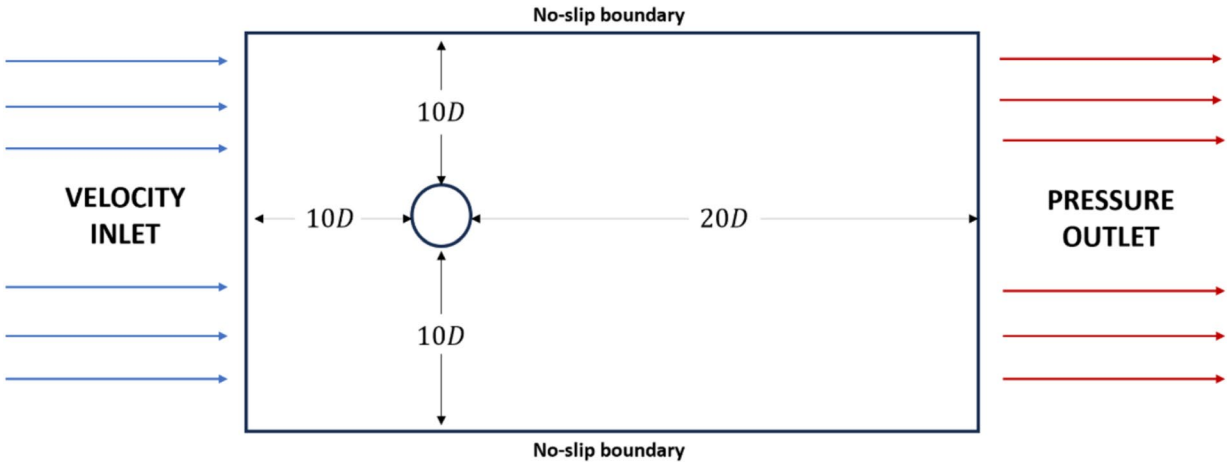


**Fig. 3** Computational domain setup

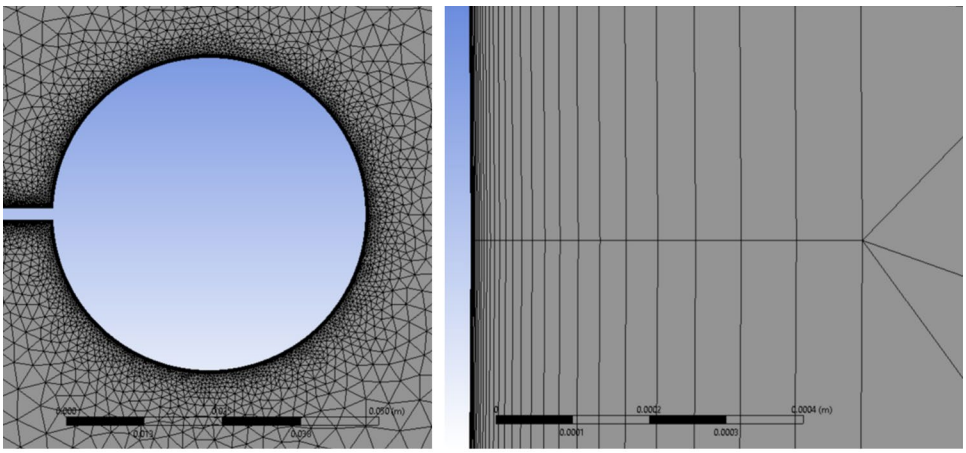

**(a)** **(b)**

**Fig. 4** Mesh generation around the bluff body: **a** triangular elements; **b** inflation layers

The CFD simulation was set up using the ANSYS Fluent 2022 R2 solver with a triangular mesh, as shown in Fig. 4a, comprising approximately 180,000 elements and 30 layers of inflation around the bluff body as displayed in Fig. 4b. A mesh independence study was conducted by comparing the computational fluid dynamics (CFD) results of the drag coefficient using three different mesh sizes: 135,500 elements for the coarse mesh, 152,000 elements for the medium mesh, and 180,000 elements for the fine mesh. The drag coefficients predicted by the fine mesh were within an appropriate residual level and were, therefore, utilized for further simulations. The unsteady state flow was solved using unsteady Reynolds-averaged Navier–Stokes equations, also known as the URANS equations. To account for turbulence and because the Reynolds number defined as $R_e = \rho \nu D/\mu$ exceeds the transition interval, a k–ω SST viscous model was utilized (Menter 1994). A time interval of 0.002 s was solved over 15 s, and 20 iterations per time step were chosen to provide adequate values for observing vortex shedding and convergence. The solver employed a semi-implicit method for the pressure-linked equations (SIMPLE) algorithm, which balances computational expense and convergence rates. Additionally, second-order upwind spatial discretization and second-order implicit transient formulation settings were applied to the simulation to solve the inner region of the boundary layer. These settings are commonly used for numerical accuracy and stability in CFD simulations. Additionally, to keep the y value positive and less than unity, which is the distance of the first node from the cylinder wall, the mesh was refined to ensure an accurate representation of the flow near the bluff body. After reaching an appropriate level of residuals, the simulation was considered converged for the variables of velocity, pressure, and turbulence.

## 3 Experimental Study

The findings from CFD simulations provide a basis for experimental validation, which is conducted to assess further the performance differences between configurations A and B under controlled wind tunnel conditions. Subsequently, a comparative analysis is conducted to assess the two distinct spatial configurations, Configuration A and Configuration B, aiming to corroborate the outcomes derived from the simulation study. Two configurations were analyzed: Configuration A, where the bluff body faces the incoming wind, and Configuration B, where it faces away. The study aimed to optimize vorticity generation to enhance turbulence and increase output voltage.

### 3.1 Harvester Design

To build the proposed system, 3D Printing was used for rapid prototyping and optimization of the harvester, as shown in Fig. 5. The piezoelectric generation comes from the bending of the beam, and the electromagnetic generation comes from the oscillation of the three suspended bar magnets. Utilizing a configuration of three bar magnets proves advantageous over a single magnet due to the resultant enhancement of magnetic flux strength. Nevertheless, it is important to restrict the number of bar magnets employed, as an excessive quantity would lead to an undesirable and impractical increase in the system's overall weight. In this context, the selection of three bar magnets represents a deliberate compromise, balancing the need for improved magnetic flux with the constraint of managing the weight.

As for the electromagnet, to suspend the bar magnets effectively, a configuration involving the placement of two disk magnets on top and four disk magnets beneath is employed. This arrangement necessitates the utilization of additional magnets beneath the bar magnets to counterbalance their weight, thereby ensuring stable suspension. Neodymium magnets were used for their exceptional magnetic strength (Yüksel 2017). In comparison to other magnet types, they exhibit the highest level of permanent magnetism, rendering them especially suitable for this application due to their capacity to provide robust magnetic support while maintaining structural integrity. To restrict the vertical oscillation of the bar magnets and facilitate controlled motion, a system incorporating two slits is employed. This arrangement serves the crucial purpose of ensuring that the magnetic flux linkage through the coils undergoes alternating changes in correspondence with the magnets' movement.

Consequently, this oscillatory action plays a pivotal role in inducing voltage generation within the electromagnetic harvester (Phan et al. 2020). As proven by Muthalif et al. (2022), when incorporating an electromagnetic core, it is observed that the highest field strength is achieved at the midpoint of the entire wire coil assembly. Introducing multiple coil stages in the proposed cores leads to establishing multiple concentration points for maximum field strength. Additionally, incorporating multiple-stage electromagnetic coils results in a more substantial flux change rate, subsequently leading to a notable increase in the output voltage. This strategic design enhancement contributes significantly to the augmentation of the hybrid harvester's overall performance. The highest voltage output was obtained while using the 3-stage coil configuration. Therefore, this configuration was employed in the design of this harvester, as can be seen in Fig. 5c. When the harvester undergoes vibration, the bar magnets oscillate relative to the coils, thereby inducing a voltage.

A three-part modular support structure was employed to secure the experimental setup in a stable position. The design of this support structure was characterized by its hollow configuration, which served a dual purpose. Firstly, the hollow design facilitated the routing of cables from the piezoelectric patch and electromagnetic harvester, allowing them to pass through the support structure, out of the wind tunnel, and connect to the BNC Cables and the Data Acquisition (DAQ) system. Secondly, the cylindrical shape of the support structure was deliberately chosen to align with the circular apertures that were in the wind tunnel section. Furthermore, this shape was also inspired by findings from a study conducted by Harimi and Saghafian (2012), which indicated that the Von Karman effect is a vortex-shedding phenomenon that is more pronounced when multiple cylindrical bodies are placed in a series. The connection between BNC channels and the Data Acquisition (DAQ) system represents a critical aspect of the experimental setup, significantly influencing the voltage output. Notably, the arrangement of these connections played a pivotal role in determining the resulting voltage levels. Specifically, parallel connections yield the lowest voltage output, while separate and series channel connections produce notably higher voltage outputs. Therefore, the decision was made to implement series connections in the design, as they offered the most advantageous voltage output configuration. In this experiment, the electromagnet and piezoelectric are connected to different BNC channels. This allows for monitoring and comparison of the effects of each channel separately.

The piezoelectric patch used in the harvester is a Macro-Fiber Composite (MFC), with an active area of 196 $mm^2$. The beam and bluff body are made of PLA with a length of 80 mm and a diameter of 50 mm, respectively. A detailed breakdown of the materials used, along with their dimensions, is presented in Table 1.

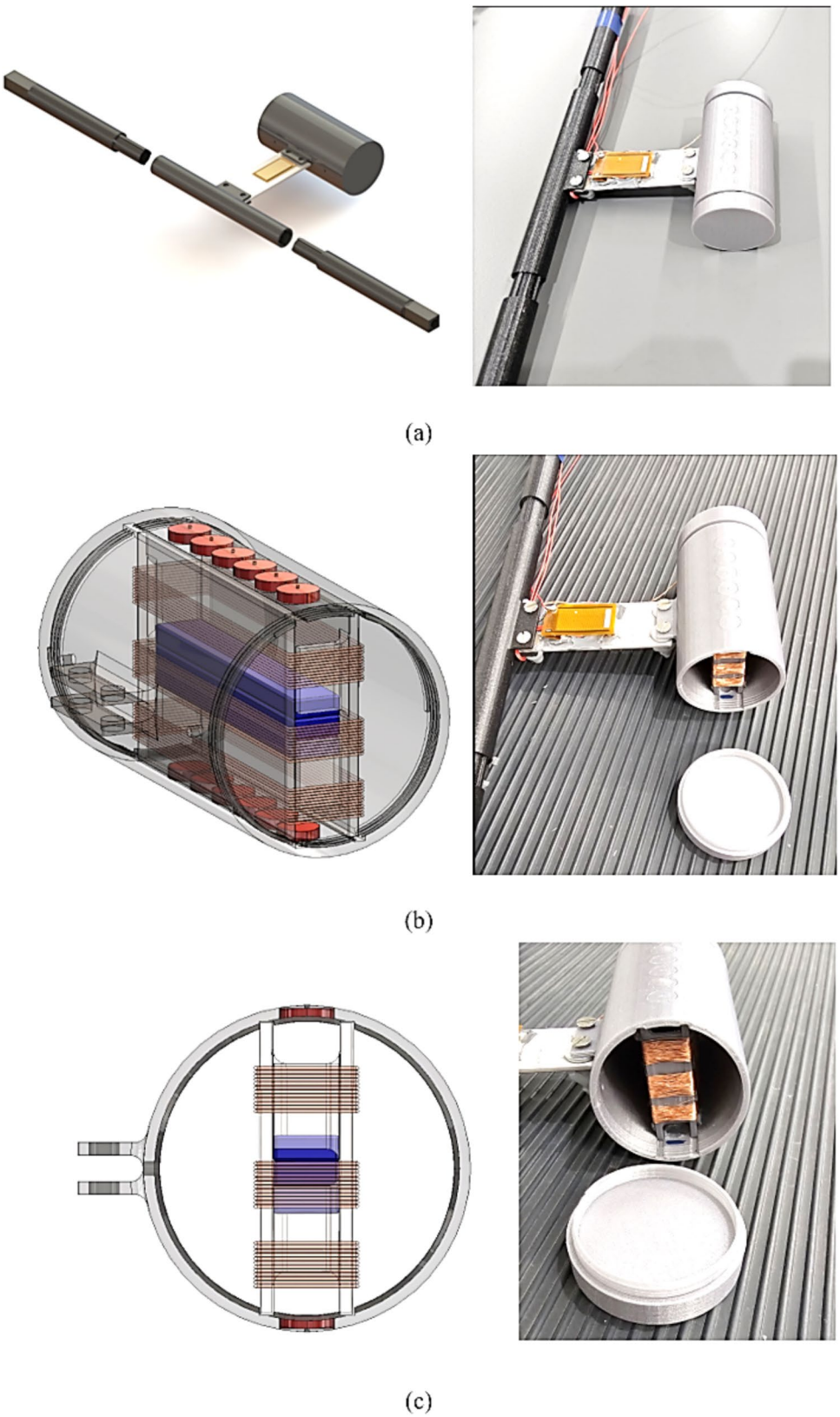


**Fig. 5** **a** External view of three-part modular support structure. **b** Internal view of harvester. **c** 3-stage coils

**Table 1** Variables and parameters of the system

| Symbol | Description | Value | Unit |
|---|---|---|---|
| D | Diameter of bluff body | 50 | mm |
| H | Height of bluff body | 50 | mm |
| L | Length of beam | 80 | mm |
| $\rho_{piezo}$ | Active piezoelectric patch density | 7800 | |
| $C_p$ | Clamp capacitance for piezoelectric transducer | – | F |
| Θ | Electromechanical coupling coefficient | – | $NV^{-1}$ |
| $A_{2807}$ | 2807-P2 piezoelectric active area | 196 | $mm^2$ |
| $D_{cm}$ | Circular Magnet diameter | 8.30 | mm |
| $t_{cm}$ | Circular Magnet thickness | 2 | mm |
| $L_{bm}$ | Bar Magnet length | 64.2 | mm |
| $h_{bm}$ | Bar Magnet height | 3 | mm |
| $w_{bm}$ | Bar Magnet width | 9.8 | mm |
| $D_c$ | Copper wire diameter | 0.4 | mm |

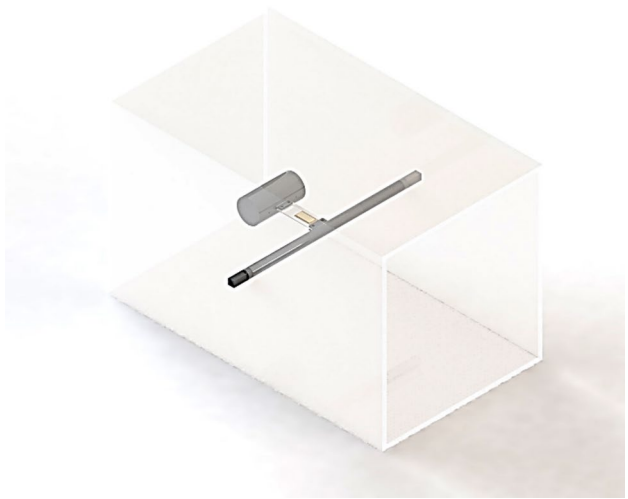

**Fig. 6** Clamping mechanism

The outer terminations of these supports were given a cuboidal form, as shown in Fig. 6, a design consideration made for practical reasons. This cuboidal geometry facilitated secure clamping and ensured the stability of the support structure, mitigating the risk of any unintended rotation. This, in turn, contributed to the overall integrity of the experimental setup by preventing potential misalignment or disturbances during the experiment. Table 1 presents the detailed dimensions and characteristics of the proposed system. Each component is measured precisely to ensure accuracy in design and functionality.

## 3.2 Experimental Setup

The wind tunnel experiment was conducted to investigate the effect of the two configurations and, consequently, vorticity formation on the harvester's performance. The experimentation took place within a subsonic wind tunnel, offering the capability to vary airflow velocity systematically. A substantial fan drove the wind tunnel's airflow, and its power was adjustable to control the airstream's velocity precisely. A deliberate spatial arrangement was adopted to ensure the validity of experimental measurements. The experimental apparatus was positioned at a distance from the wind tunnel inlet, allowing for the establishment of a fully developed flow within the channel. Furthermore, it was strategically situated away from the tunnel walls, a precaution taken to prevent any confounding effects attributable to wall interactions. The synchronization process was implemented experimentally by adjusting the tip mass in increments of 5 g to tune the natural frequency of the system. The parameter range for tuning spanned from 2 to 10 Hz, ensuring alignment with the vortex-shedding frequency under varying wind speeds. The wind tunnel experiments were conducted at wind speeds ranging from 2 m/s to 9 m/s, with a focus on the synchronization region around 5 m/s, which corresponds to the natural frequency of the system. The experimental setup ensured fully developed flow conditions, with the harvester positioned centrally within the wind tunnel to minimize wall effects.

A data acquisition system was used to measure the voltage output from the piezoelectric patch and the electromagnetic harvester, as illustrated in Fig. 7 and the schematic diagram in Fig. 8, which shows the developed prototype with fully integrated components. For this purpose, the Dewesoft Sirius data acquisition (DAQ) device was utilized in conjunction with the DewesoftX software. Each recording lasted for 30 s after achieving a steady flow at the natural frequency of the system. The time-domain data were converted into a graphical plot using Fast Fourier transform (FFT) analysis with a Hanning window and a resolution of 0.1 Hz at a sampling frequency of 5000 Hz. This was used to create an average graphical depiction of the time-domain response using FFT analysis. The linear peaks, averaging over the entire period with an overlap average of 66.7%, were recorded in the frequency domain analysis. To minimize missing or unevenly weighted parts of the time signal, a larger overlap and windowing approach were employed to ensure that every sample in the time domain was accurately accounted for in the frequency domain (Trethewey 2000; Nguyen 2021).

Figure 9 shows a signal block diagram illustrating a process flow where mechanical vibrations caused by fluid flow are captured using two types of sensors (Piezoelectric and Electromagnetic).

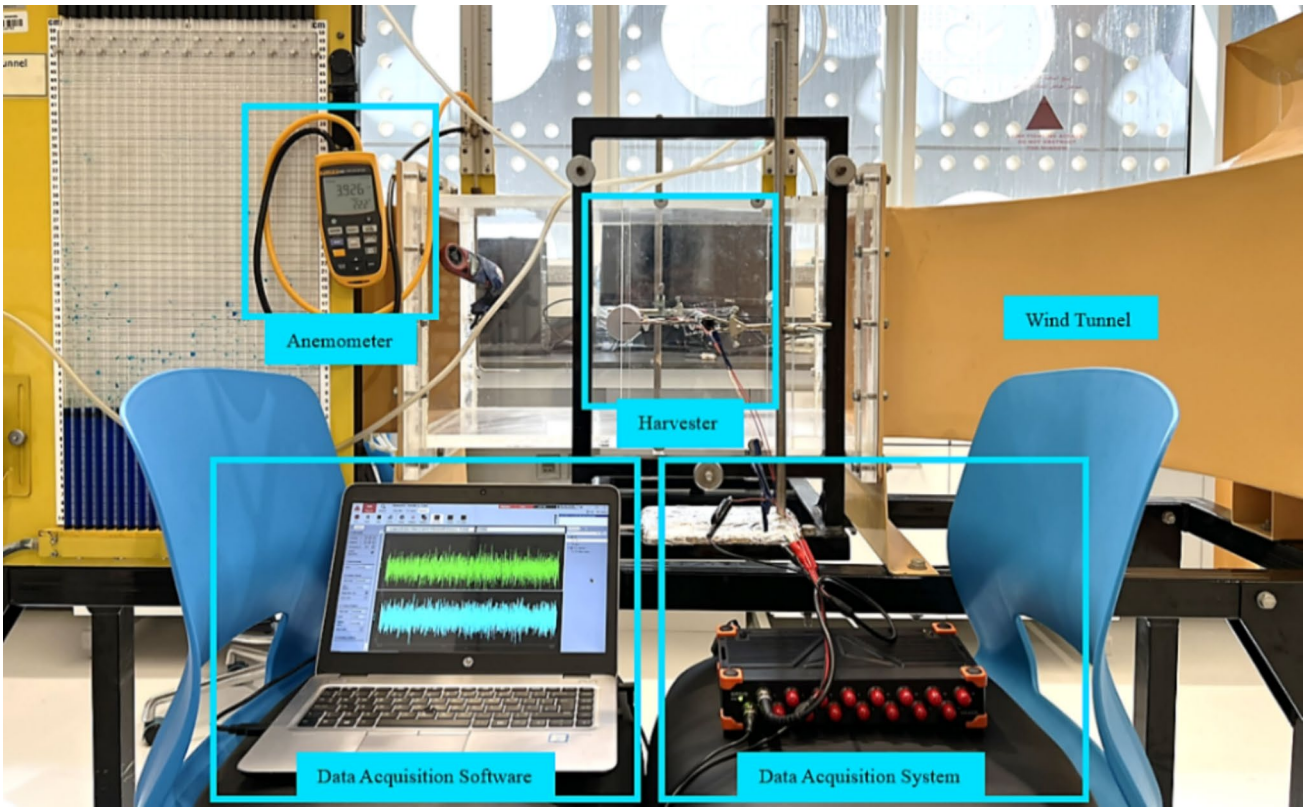


**Fig. 7** Experimental setup

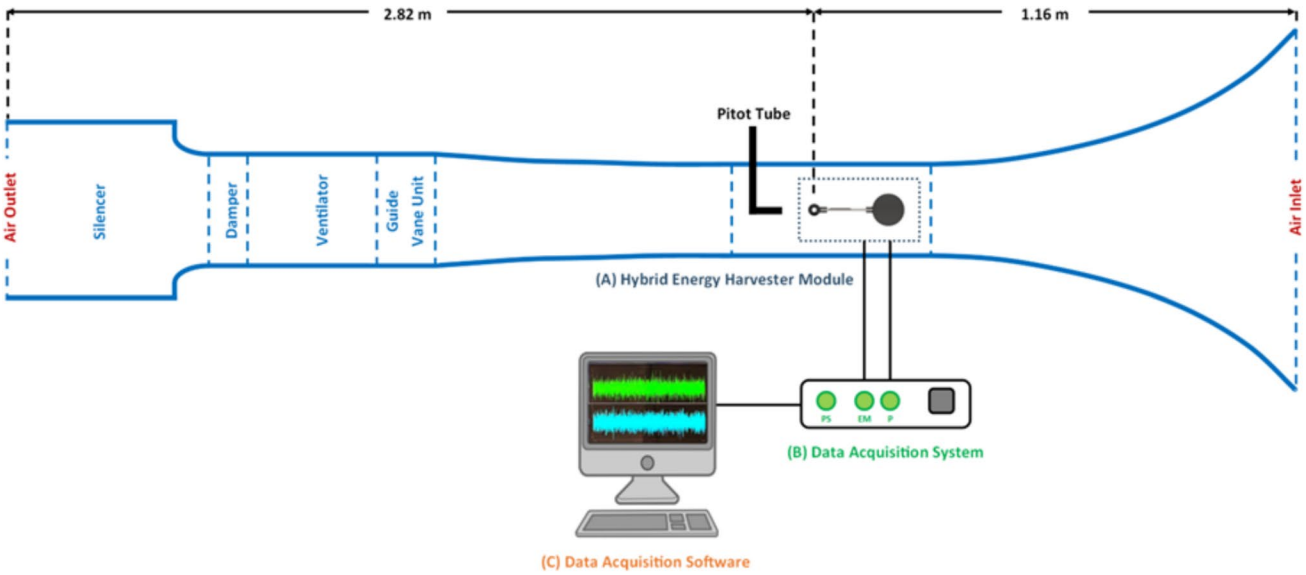


**Fig. 8** Schematic of experimental setup

The signals from these sensors are digitized by a DAQ system and then analyzed using signal processing techniques, including time-domain analysis and FFT. Figure 10 provides a visual comparison of two different experimental setups: Configuration A (Fig. 10a) and Configuration B (Fig. 10b), allowing for analysis of how changing the configurations impacts the outcomes. This comparison was

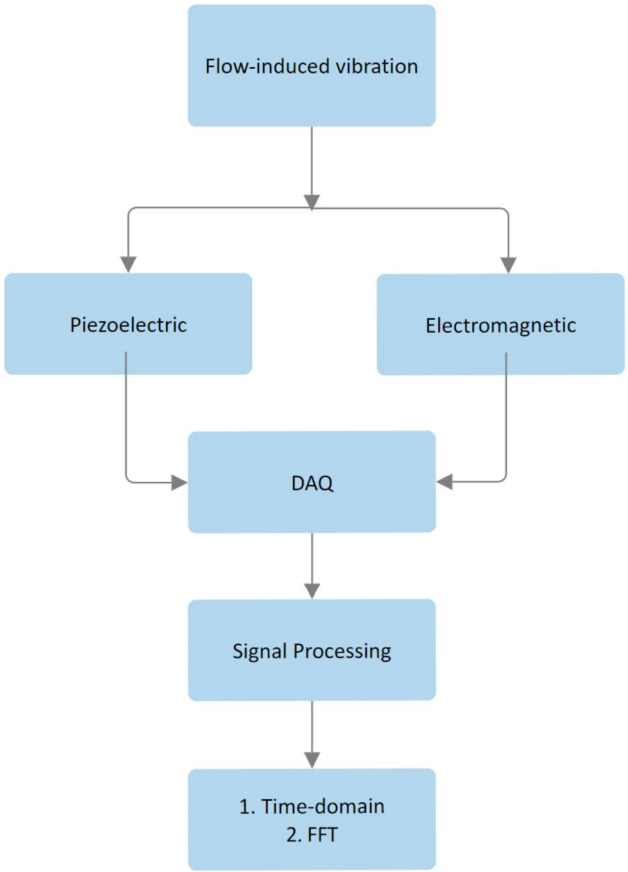


**Fig. 9** Signal block diagram

done to understand the robustness of the experiment and to identify the optimal setup for the desired outcomes.

## 4 Results and Discussions

### 4.1 CFD Results

Two different configurations, as depicted in Fig. 11, were subjected to comparative analysis. Configuration A is characterized by the orientation of the bluff body facing the incoming wind, while Configuration B is characterized by the bluff body facing away from the incoming wind. The primary objective of this study is to optimize vorticity generation and, consequently, enhance turbulence and, thus, output voltage.

To accomplish this goal, an external flow computational fluid dynamics (CFD) simulation was conducted to explore the distribution and interaction of fluid flow around and downstream of the bluff body, operating under a wind speed of 5 m/s, which closely represents the average wind speed in Qatar. This comprehensive investigation utilized velocity contours and plots of turbulent kinetic energy to facilitate a detailed comparison of the two configurations. The results of this CFD simulation are presented in Fig. 12, which provides valuable insights into the flow dynamics and turbulence characteristics associated with each configuration.

The simulation involved assessing the localized turbulent kinetic energy in the vicinity of the cylindrical bluff body and beam setup when exposed to fluid flow in proximity to the synchronization region. Turbulence generation in this study is primarily attributed to abrupt changes in the geometry of the experimental setup, primarily induced by the presence of the cylindrical bluff body. It's noteworthy to mention that the diameter of the bluff body remains consistent across both configurations, with the primary distinction residing in their relative positioning compared to the beam.

In Configuration A, the positioning of the beam downstream of the cylinder results in the absorption of some vortices produced by the bluff body. This effectively prevents the free formation of vortices in the immediate wake of the cylinder. Conversely, Configuration B employs a setup where the beam is placed upstream of the cylinder, creating an unobstructed downstream region free of geometric interference. This arrangement facilitates the unimpeded formation of vortices, as visually depicted in Fig. 12a–d. Furthermore, Fig. 12d illustrates that Configuration B exhibits notably higher levels of turbulent kinetic energy due to the unhindered vorticity generation. Additionally, it is of significance to highlight that within Configuration B, the point of maximum turbulence is located downstream, a feature that supports the generation of vortices. Conversely, in Configuration A, this maximum turbulence occurs in the immediate vicinity of the beam because of interference effects.

The quantitative analysis underscores the disparity in turbulence levels between the two configurations. Configuration B exhibits a 33% higher turbulent kinetic energy (TKE) of 2.8 $m^2/s^2$ compared to Configuration A's 2.1 $m^2/s^2$, highlighting its superior ability to enhance fluid–structure interactions. This substantial increase in TKE can be attributed to the unobstructed formation and evolution of vortices around the bluff body, enabled by the optimized spatial arrangement in Configuration B. By minimizing wake interference and allowing vortices to shed more freely and symmetrically, Configuration B sustains stronger and more coherent flow instabilities. These intensified turbulent structures result in greater oscillatory motion, thereby increasing the mechanical strain experienced by the energy harvesting elements. As a result, the system demonstrates improved aerodynamic performance and yields a higher voltage output, affirming the critical role of spatial configuration in maximizing the efficiency of vortex-induced energy harvesters.

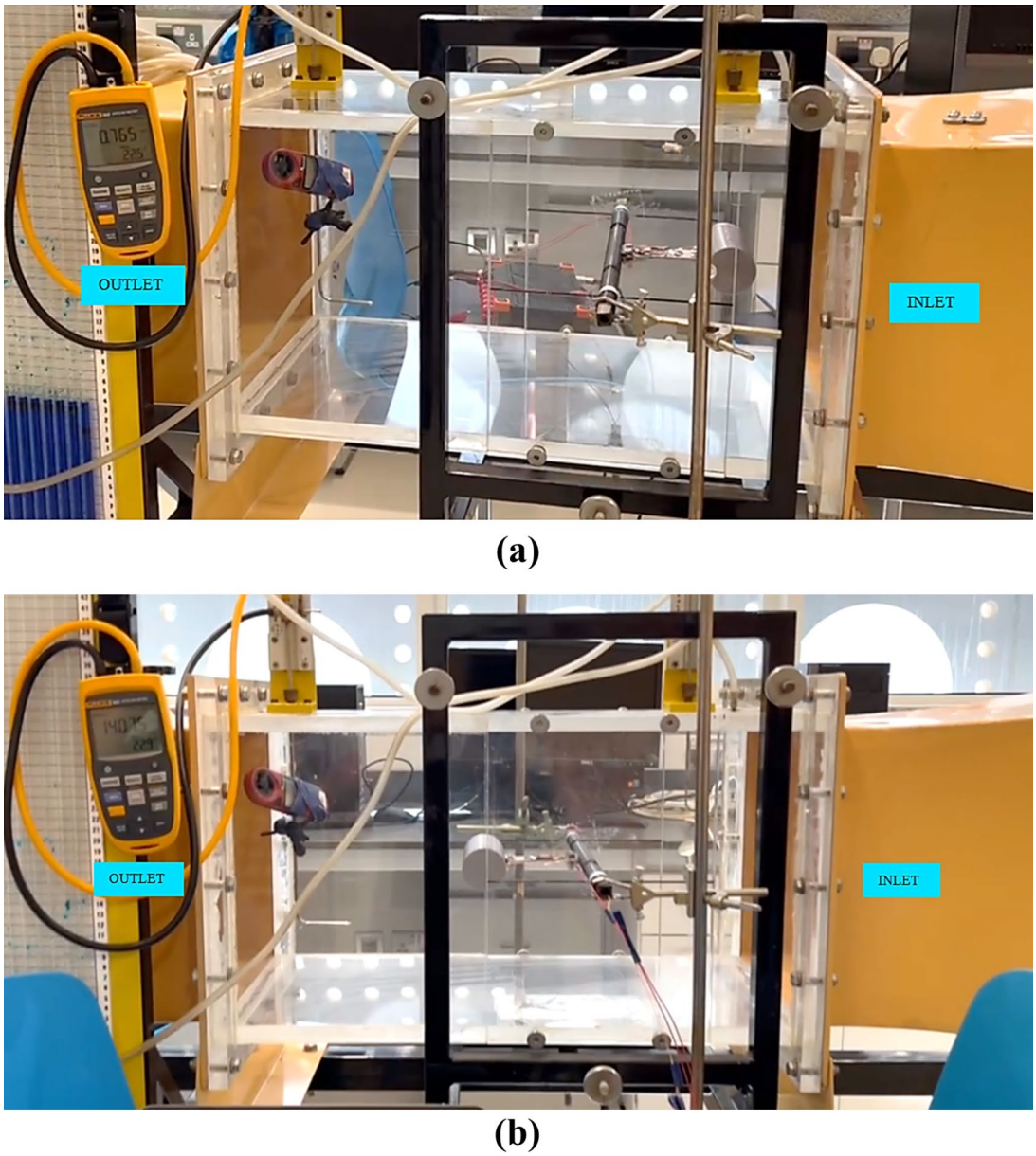


**Fig. 10** Experimental setup: **a** Configuration A; **b** Configuration B

## 4.2 Synchronization

The comparison of vibration differences is emphasized in Fig. 13, providing an insight into the differences observed before, during, and after synchronization. During synchronization, a noteworthy phenomenon occurs when the vortex-shedding frequency closely aligns with or matches the structural natural frequency within still air conditions. This alignment results in a substantial increase in vibration amplitude, similar to the characteristics of resonance typically exhibited by vibration-based energy harvesters. In contrast to the pre-synchronization phase, where the overall output voltage is relatively low, and the post-synchronization period, which displays a dip in voltage output, the synchronization region oscillations are distinctive as they have more energy and continuous high voltage output, a consequence of the positive feedback loop between the system's natural frequency and vortex shedding. This phenomenon is particularly significant in the context of energy harvesting due to its ability to sustain elevated voltage levels. The effect of synchronization observed in this study is also applicable to regular piezoelectric harvesters (PEH). A 60-s time interval for data collection is used across all wind speeds to ensure that the system reaches a steady-state condition, minimizing the influence of initial transient effects.

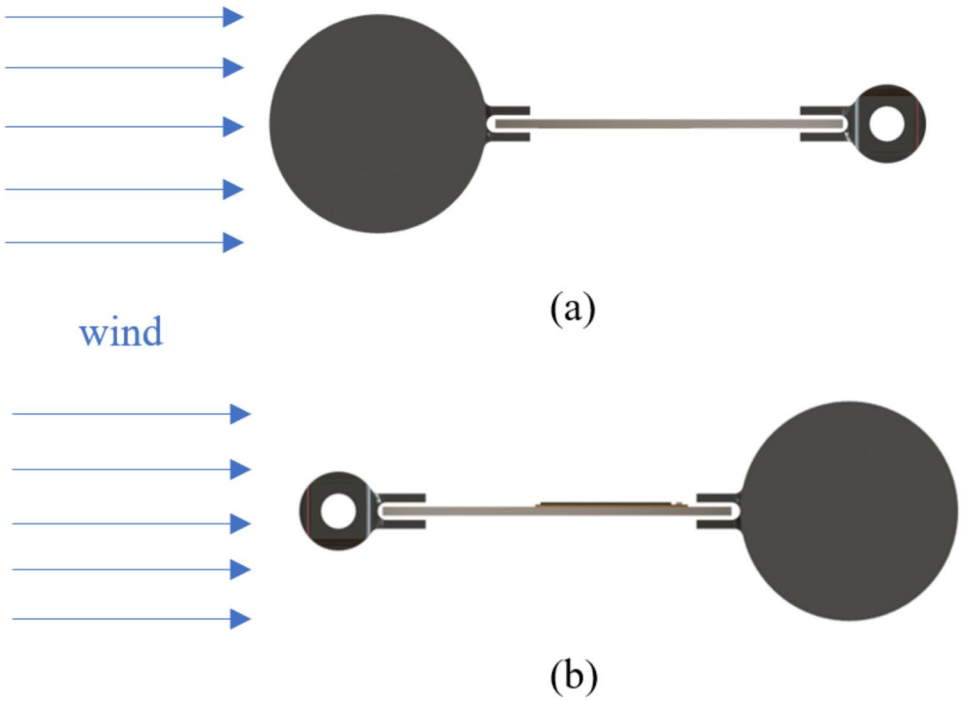


**Fig. 11** **a** Configuration A; **b** Configuration B

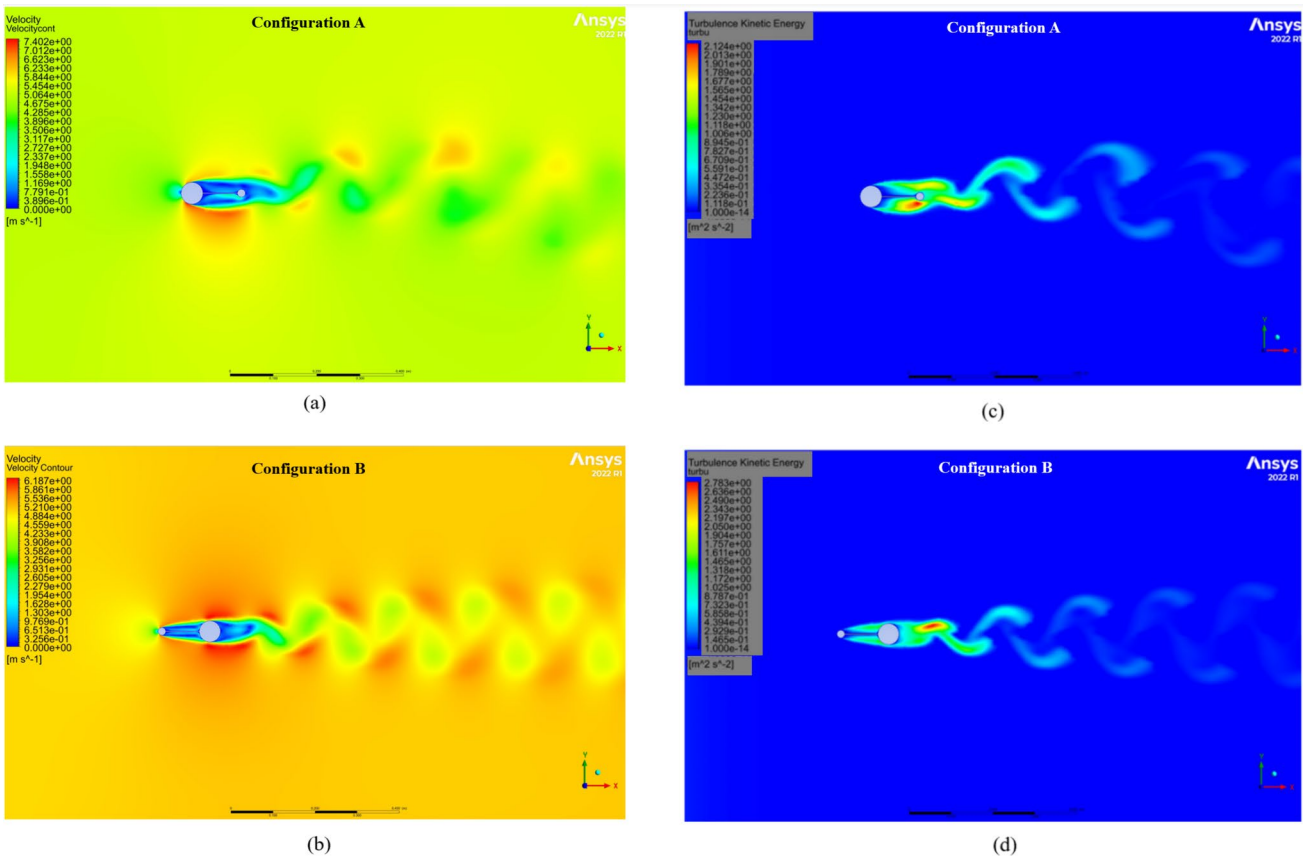


**Fig. 12** Flow distribution plots of Configuration A (**a**) Velocity, (**b**) Turbulence, and for Configuration B (**c**) Velocity, (**d**) Turbulence

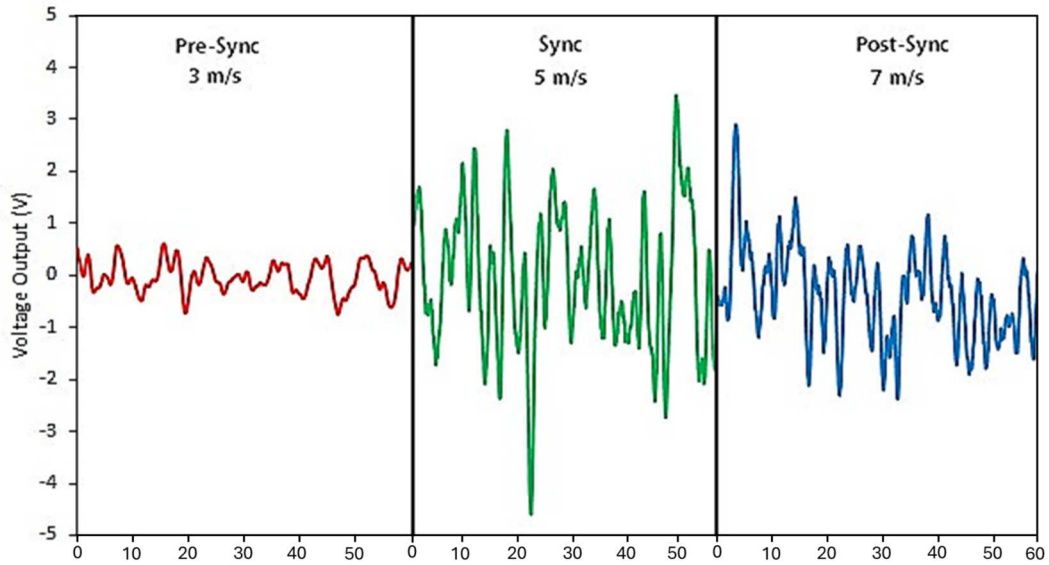


**Fig. 13** Time-domain synchronization effects of hybrid harvester

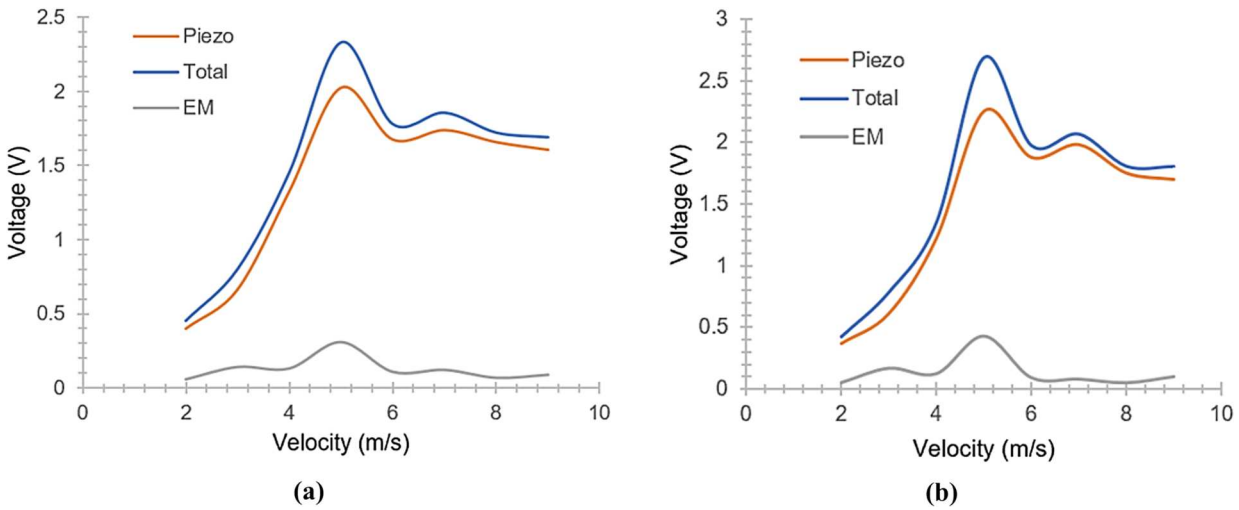


**Fig. 14** Voltage Distribution for **a** Configuration A; **b** Configuration B

### 4.3 RMS Voltage Performance Analysis

Figure 14 shows that the voltage output in the hybrid piezoelectric-electromagnetic harvester is higher than that of an individual piezoelectric harvester due to the combined utilization of piezoelectric and electromagnetic mechanisms. This combination allows for enhanced energy conversion efficiency and increased power generation capabilities. The hybrid configuration has about 20% higher voltage output than piezo alone.

The performance analysis of the two hybrid energy harvester configurations is presented in Fig. 15, where the velocity was increased from 2 to 9 m/s, and the Root Mean Square (RMS) voltage values, as well as Eq. (8), were employed at various wind speeds to construct the graphical representation. Notably, the influence of the synchronization region is apparent, characterized by a peak in voltage output occurring in proximity to the structural natural frequency. This occurs at a velocity of about 5 m/s. This is the speed at which the vortex shedding frequency matches the structural natural frequency. It is within 20% of the predicted value of 4.2 m/s as calculated using Eq. (7). This comparison reveals that Configuration B exhibits a 15% higher voltage output than Configuration A during the synchronization region. Furthermore, Configuration B maintains an elevated voltage output beyond the lock-in region, thus indicating its

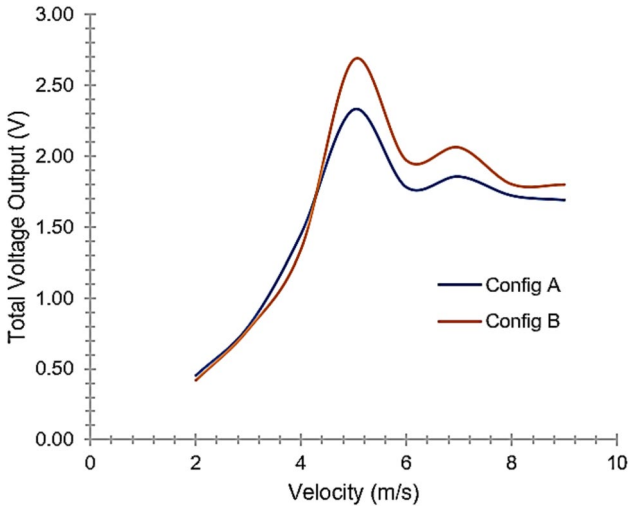


**Fig. 15** Performance analysis at different wind speeds

sustained performance advantage. This empirical observation underscores the significance of optimal configuration in maximizing energy harvesting performance. This improvement is attributed to the absence of wake interference, which allows for a more stable and periodic vortex street, thereby maximizing energy transfer efficiency during synchronization (Bearman 2011; Zhao 2023). Prior studies have shown that similar experiments typically report uncertainty margins of $\pm 10\%$ for RMS voltage measurements.

### 4.4 Frequency Domain Analysis

The comparative assessment of the two hybrid harvester configurations can be extended into the frequency domain, as illustrated in Fig. 16. A notable attribute in both configurations is the distinct peak occurring at resonance, corresponding to the system's natural frequency. The region conducive to energy harvesting, which is depicted as the harvestable zone, pertains to an elastically mounted cylinder oscillating due to vortex-induced vibrations within the frequency range of 5–8 Hz. Even beyond the resonance peak, Configuration B consistently maintains a higher voltage output than Configuration A within this region. Andrianne et al. (2018) emphasized that VIV-based harvesters must generate a power output ranging from micro to 15 milliwatts to effectively supply energy for sensors and MEMS devices, which can be obtained from this system. Moreover, because of the low-frequency measurements up to 10 Hz and the energy harvester design optimized for this range, the ability to improve bandwidth performance is restricted by the resolution of the data acquisition system.

The narrowband performance observed here is a characteristic feature of a beam-coupled system, distinguished by its specific natural mode shape. It is important to note that an increase in the number of bar magnets would result in a higher mass for the electromagnetic system, consequently raising the overall mass of the harvester and thereby shifting the system toward a lower natural frequency. This, in turn, presents the potential for energy harvesting applications within low-velocity wind flow scenarios.

## 5 Conclusions

This research introduces a hybrid energy harvesting system integrating piezoelectric and electromagnetic mechanisms. It compares two distinct configurations in the context of incoming wind flow, focusing on the significance of avoiding geometrical interference in the wake region of a bluff body to enhance turbulence. The core of the energy harvesting system involves a bluff body that internally houses

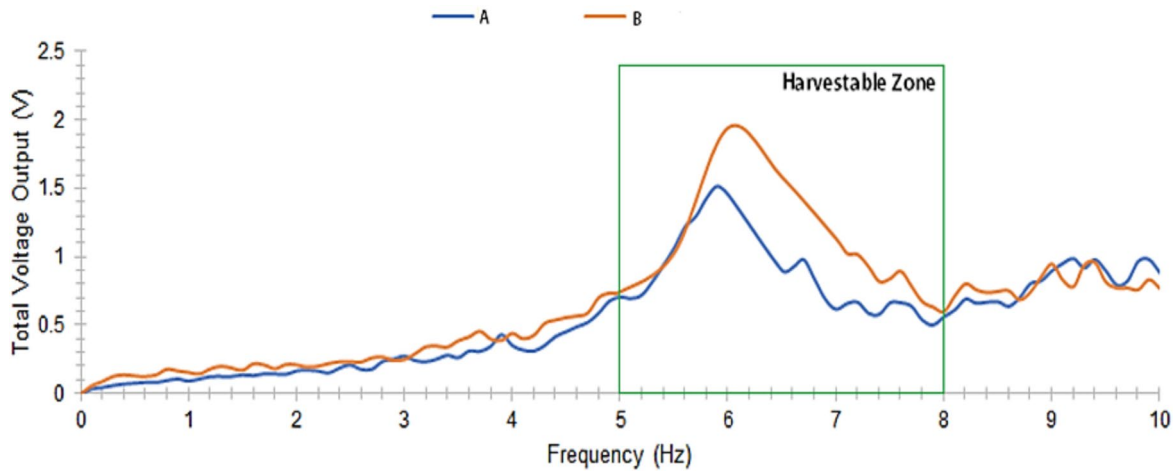


**Fig. 16** Velocity-averaged voltage output frequency domain for the two harvester configurations

floating permanent magnets, creating oscillations within a coil to induce voltage through fluctuations in magnetic flux. Additionally, a piezoelectric macro-fiber composite affixed to a beam substrate generates electricity by exploiting mechanical strain. Both configurations of this hybrid system are realized through the innovative utilization of 3D printing technology, which offers rapid prototyping capabilities and adaptability for iterative adjustments. A comprehensive simulation study is conducted to compare the turbulent energy generated within the two distinct configurations. Subsequently, experimental assessments are undertaken within a subsonic wind tunnel encompassing a range of variable wind speeds. The key findings of this study are as follows:

1. A hybrid piezoelectric-electromagnetic system can harvest energy from wind flow and be tuned for low-velocity use in environmental monitoring. It provides power to sensors that collect data on temperature, humidity, or pollution levels.
2. The hybrid configuration has about 20% higher voltage output than piezo alone.
3. In Configuration A, introducing a beam structure within the wake region disrupts the formation of vortices, hindering their complete development and leading to irregular vortex shedding. This interference reduces the von Kármán effect, which is a critical component of efficient energy harvesting from vortex-induced vibrations.
4. A notable enhancement is observed in Configuration B, characterized by the absence of obstructive geometrical features in the wake section of the bluff body, with a remarkable 33% increase in turbulent kinetic energy compared to Configuration A. This outcome is attributed to the unimpeded formation of vortices and the absence of interference posed by the beam present in the wake section of Configuration A.
5. During the synchronization phase, Configuration B demonstrates a substantial performance advantage by generating 15% more voltage output than Configuration A. Furthermore, Configuration B maintains this superior voltage output throughout the post-synchronization period.

The findings in this work have demonstrated the importance of choosing the correct spatial configuration when using energy harvesters. The results highlight the importance of unobstructed wake regions in energy harvesting configurations. Configuration B's superior performance in terms of turbulent kinetic energy and voltage output reinforces the significance of design choices in maximizing energy harvesting efficiency. The enhanced performance observed in this study, where uninterrupted vorticity formation prevails, holds promise for enhancing the viability of self-sustaining wireless sensors. Moreover, the potential for low-velocity energy harvesting is evident, and it can be accomplished through cost-effective and scalable methods facilitated by additive manufacturing techniques such as 3D printing. In future research, an additional investigation could be undertaken to explore the correlation between the beam's width and its impact on voltage output.

**Acknowledgements** This work was supported by Qatar University – Student Grant no. QUST-1-CENG-2023-85, and Open Access funding is provided by the Qatar National Library (QNL).

**Author Contributions** Abdul Saboor: Data Curation, Investigation, Analysis, Methodology, Experimental Work, Writing – Draft, Review and Editing, Kangokar Nithin: Data Curation, Experimental Work, Writing – Review and Editing, Muhammad Hafizh: Methodology, Experimental Work, Writing – Review & Editing, Mohammad Farhan: Visualization, Validation, Reviewing and Editing, Asan G. A. Muthalif: Conceptualization, Methodology, Visualization, Investigation, Supervision, grant acquisition, Validation, Writing- Reviewing and Editing.

**Funding** Open Access funding provided by the Qatar National Library.

**Data Availability** Data is provided within the manuscript.

## Declarations

**Conflict of Interest** The authors declare no competing interests.



## References

Akaydin HD, Elvin N, Andreopoulos Y (2012) The performance of a self-excited fluidic energy harvester. Smart Mater Struct. https://doi.org/10.1088/0964-1726/21/2/025007

Andrianne T et al (2018) Energy harvesting from different aeroelastic instabilities of a square cylinder. J Wind Eng Ind Aerodyn. https://doi.org/10.1016/j.jweia.2017.10.031

Bearman PW (2011) Circular cylinder wakes and vortex-induced vibrations. J Fluids Struct. https://doi.org/10.1016/j.jfluidstructs.2011.03.021

Beeby SP, Tudor MJ, White NM (2006) Energy harvesting vibration sources for microsystems applications. Meas Sci Technol. https://doi.org/10.1088/0957-0233/17/12/R01

Blevins RD (2009) Models for vortex-induced vibration of cylinders based on measured forces. J Fluids Eng Trans ASME. https://doi.org/10.1115/1.3222906

Chakhari J, Nasraoui MT, Mrad C, Khalfi B (2023) Design and modeling of piezoelectric energy harvester under variable pressure in pipe flow. Iran J Sci Technol Trans Mech Eng. https://doi.org/10.1007/s40997-022-00541-w

Challa VR, Prasad MG, Fisher FT (2009) A coupled piezoelectric-electromagnetic energy harvesting technique for achieving increased power output through damping matching. Smart Mater Struct. https://doi.org/10.1088/0964-1726/18/9/095029

Dalton C (2010) A review of vortex-induced vibrations. In: Proceedings of the 12th International Conference on Engineering, Science, Construction, and Operations in Challenging Environments-Earth and Space. https://doi.org/10.1061/41096(366)198

Elahi H, Eugeni M, Gaudenzi P (2018) A review on mechanisms for piezoelectric-based energy harvesters. Energies. https://doi.org/10.3390/en11071850

Esalat H, Shooshtari A, Karami H (2023) Analytical modeling for energy harvesting of lateral vibrations of rotating machines via electromagnetic mechanisms. Iran J Sci Technol Trans Mech Eng. https://doi.org/10.1007/s40997-022-00490-4

Facchinetti ML, de Langre E, Biolley F (2004) Coupling of structure and wake oscillators in vortex-induced vibrations. J Fluids Struct. https://doi.org/10.1016/j.jfluidstructs.2003.12.004

Fakhzan MN, Muthalif AGA (2013) Harvesting vibration energy using piezoelectric material: modeling, simulation and experimental verifications. Mechatronics 23:61–66

Farhan M, Muthalif AGA, Ali MSM (2024) Innovative approaches to optimize vibration energy harvesting (VEH): a comprehensive review. Energy Rep 12:5194–5219

Franzini GR, Bunzel LO (2018) A numerical investigation on piezoelectric energy harvesting from Vortex-Induced Vibrations with one and two degrees of freedom. J Fluids Struct. https://doi.org/10.1016/j.jfluidstructs.2017.12.007

Gabbai RD, Benaroya H (2005) An overview of modeling and experiments of vortex-induced vibration of circular cylinders. J Sound Vib. https://doi.org/10.1016/j.jsv.2004.04.017

Gao X, Shih WH, Shih WY (2013) Flow energy harvesting using piezoelectric cantilevers with cylindrical extension. IEEE Trans Ind Electron. https://doi.org/10.1109/TIE.2012.2187413

Hafizh M et al (2021) A hybrid piezoelectric-electromagnetic nonlinear vibration energy harvester excited by fluid flow. Compt Rend Mec 349:65–81

Harimi I, Saghafian M (2012) Numerical simulation of fluid flow and forced convection heat transfer from tandem circular cylinders using overset grid method. J Fluids Struct. https://doi.org/10.1016/j.jfluidstructs.2011.12.006

Ibrahim DS, Muthalif AGA, Nordin NHD, Saleh T (2017) Comparative study of conventional and magnetically coupled piezoelectric energy harvester to optimize output voltage and bandwidth. Microsyst Technol 23:2663–2674

Jia J et al (2018) Modeling and analysis of upright piezoelectric energy harvester under aerodynamic vortex-induced vibration. Micromachines. https://doi.org/10.3390/mi9120667

Jiang H et al (2020) VDF-content-guided selection of piezoelectric P(VDF-TrFE) films in sensing and energy harvesting applications. Energy Convers Manag. https://doi.org/10.1016/j.enconman.2020.112771

Kianpoor A, Jahani K (2019) Modeling and analyzing of energy harvesting from trapezoidal piezoelectric beams, Iran. J Sci Technol Trans Mech Eng. https://doi.org/10.1007/s40997-018-0154-0

Konstantinidis E, Dorogi D, Baranyi L (2021) Resonance in vortex-induced in-line vibration at low Reynolds numbers. J Fluid Mech. https://doi.org/10.1017/jfm.2020.850

Lai Z et al (2021) A hybrid piezo-dielectric wind energy harvester for high-performance vortex-induced vibration energy harvesting. Mech Syst Signal Process. https://doi.org/10.1016/j.ymssp.2020.107212

Lin H et al (2019) Angle-shaped triboelectric nanogenerator for harvesting environmental wind energy. Nano Energy. https://doi.org/10.1016/j.nanoen.2018.11.037

Lu C et al (2021) Gear rotational speed sensor based on FeCoSiB/Pb(Zr, Ti)$O_3$ magnetoelectric composite. Meas J Int Meas Confed. https://doi.org/10.1016/j.measurement.2020.108409

Menter FR (1994) Two-equation eddy-viscosity turbulence models for engineering applications. AIAA J. https://doi.org/10.2514/3.12149

Muthalif AGA, Nordin NHD (2015) Optimal piezoelectric beam shape for single and broadband vibration energy harvesting: Modeling, simulation and experimental results. Mech Syst Signal Process 54:417–426

Muthalif AGA, Hafizh M, Renno J, Paurobally MR (2021) An enhanced hybrid piezoelectric–electromagnetic energy harvester using dual-mass system for vortex-induced vibrations. JVC/Journal Vib Control 27:2848–2861

Muthalif AGA, Hafizh M, Renno J, Paurobally MR (2022) A hybrid piezoelectric-electromagnetic energy harvester from vortex-induced vibrations in fluid-flow; the influence of boundary condition in tuning the harvester. Energy Convers Manag 256:115371

Nguyen TQ (2021) Separation of the structure signal by the maximal overlap discrete wavelet transform and fast fourier transform. Adv Mater Sci Eng. https://doi.org/10.1155/2021/3328684

Nishi Y, Shigeyoshi Y (2022) Vortex- and wake-induced vibrations of a circular cylinder placed in the proximity of two fixed cylinders. J Vib Eng Technol. https://doi.org/10.1007/s42417-021-00430-7

Norberg C (2003) Fluctuating lift on a circular cylinder: Review and new measurements. J Fluids Struct. https://doi.org/10.1016/S0889-9746(02)00099-3

Phan TN, Bader S, Oelmann B (2020) Performance of an electromagnetic energy harvester with linear and nonlinear springs under real vibrations. Sens (Switzer). https://doi.org/10.3390/s20195456

Pobering S, Ebermeyer S, Schwesinger N (2009) Generation of electrical energy using short piezoelectric cantilevers in flowing media. In: Active and Passive Smart Structures and Integrated Systems. https://doi.org/10.1117/12.815189

Pradeesh EL, Udhayakumar S (2019) Effect of placement of piezoelectric material and proof mass on the performance of piezoelectric energy harvester. Mech Syst Signal Process. https://doi.org/10.1016/j.ymssp.2019.05.044

Roundy S, Wright PK (2004) A piezoelectric vibration based generator for wireless electronics. Smart Mater Struct. https://doi.org/10.1088/0964-1726/13/5/018

Safaei M, Sodano HA, Anton SR (2019) A review of energy harvesting using piezoelectric materials: state-of-the-art a decade later (2008–2018). Smart Mater. Struct. 28:113001

Shirazi E, Jafari AA (2024) Piezoelectric energy harvesting from nonlinear vibrations of rotating system: theoretical and experimental studies. Iran J Sci Technol Trans Mech Eng. https://doi.org/10.1007/s40997-023-00731-0

Sodano HA, Inman DJ, Park G (2005) Generation and storage of electricity from power harvesting devices. J Intell Mater Syst Struct. https://doi.org/10.1177/1045389X05047210

Song R, Shan X, Li J, Xie T (2016) Modeling and experimental study of piezoelectric energy harvester under vortex-induced vibration. Hsi-an Chiao Tung Ta Hsueh/Journal Xi'an Jiaotong Univ. https://doi.org/10.7652/xjtuxb201602010

Tran MQ et al (2022) Reliable deep learning and IoT-Based monitoring system for secure computer numerical control machines against cyber-attacks with experimental verification. IEEE Access. https://doi.org/10.1109/ACCESS.2022.3153471

Trethewey MW (2000) Window and overlap processing effects on power estimates from spectra. Mech Syst Signal Process. https://doi.org/10.1006/mssp.1999.1274

Wang W, Duan P (2024) Vortex-induced vibration response of the cylinder inspired by Terebridae. Mar Struct. https://doi.org/10.1016/j.marstruc.2024.103575

Williamson CHK, Govardhan R (2008) A brief review of recent results in vortex-induced vibrations. J Wind Eng Ind Aerodyn. https://doi.org/10.1016/j.jweia.2007.06.019

Yüksel C (2017) The use of neodymium magnets in healthcare and their effects on health. North Clin Istanbul. https://doi.org/10.14744/nci.2017.00483

Zhang LB, Abdelkefi A, Dai HL, Naseer R, Wang L (2017) Design and experimental analysis of broadband energy harvesting from vortex-induced vibrations. J Sound Vib. https://doi.org/10.1016/j.jsv.2017.07.029

Zhao M (2023) A review of recent studies on the control of vortex-induced vibration of circular cylinders. Ocean Eng. https://doi.org/10.1016/j.oceaneng.2023.115389

Zhao J, Zhang H, Su F, Yin Z (2017) A novel model of piezoelectric- electromagnetic hybrid energy harvester based on vortex-induced vibration. In: Proceedings of 2017 International Conference on Green Energy and Applications, ICGEA 2017. https://doi.org/10.1109/ICGEA.2017.7925464.